

# Quantum simulation of wave optics in weakly inhomogeneous media using block-encoding

Siavash Davani,<sup>1,2,\*</sup> Martin Gärttner,<sup>3,†</sup> and Falk Eilenberger<sup>4,1,2,‡</sup>

<sup>1</sup>*Institute of Applied Physics, Abbe Center of Photonics, Friedrich Schiller University Jena, 07745 Jena, Germany*

<sup>2</sup>*Max Planck School of Photonics, 07745 Jena, Germany*

<sup>3</sup>*Institute of Condensed Matter Theory and Optics, Friedrich-Schiller-University Jena, 07743 Jena, Germany*

<sup>4</sup>*Fraunhofer-Institute for Applied Optics and Precision Engineering IOF, 07745 Jena, Germany*

(Dated: March 31, 2026)

We propose a quantum algorithm that simulates the propagation of a light field through a weakly inhomogeneous medium. The wave equation in the paraxial approximation in inhomogeneous material takes the form of the Schrödinger equation with a time-dependent Hamiltonian. This reduction is used to simulate wave optical dynamics on a quantum computer. Beam propagator operators for a short propagation distance are constructed using an efficient and flexible block-encoding that enables the simulation of various optical setups. The algorithm is showcased by simulating the propagation of a 1D Gaussian beam through a lens with a finite thickness, and the resulting spherical aberrations are demonstrated.

Keywords: Quantum algorithm, Wave optics, Hamiltonian simulation

## I. INTRODUCTION

In recent years, quantum computers have received significant attention because of their potential to advance various fields and technologies including simulation [1, 2], cryptography and communications [3], machine learning [4], and many more [5–9]. In particular, the simulation of physical systems was among the very first proposed applications of quantum computers [10] and has remained central to quantum computing research ever since [11, 12].

Quantum algorithms have been introduced for solving linear systems [13] and differential equations [14]. In some cases, these algorithms can exponentially improve the performance of simulations compared to their classical counterparts [5], once a fault-tolerant quantum computer is available [15–18]. On the algorithmic side, much work has been done on fundamental primitives such as linear combination of unitaries (LCU) [19], qubitization [20], quantum signal processing (QSP), and quantum singular value transformation (QSVT) [21]. These efforts have converged to a unified formalism [22], gathering many of the currently discovered quantum algorithms under one common framework using the notion of block-encoding [20]. Quantum signal processing using block-encoding has been proved to achieve optimal computational complexity in the time-independent Hamiltonian simulation problem [20, 21].

Nevertheless, a robust quantum algorithm for simulating wave optics has not been proposed so far. The diverse applications of wave propagation algorithms range from designing optical waveguides, lasers, and integrated circuits, to biomedical optics and imaging [23–27]. In modern optical engineering, there is an increasing need for more accurate simulations of beam propagation in complex structures where the precise control of light is essential. These simulations require significant memory and processing power, thus improving their performance is highly desired [28–30]. Quantum computers are potential candidates to reduce these computational costs. Quantum registers store a field discretized at  $N$  spatial points in only  $\log_2 N$  number of qubits. This efficiency in storage can potentially lead to exponential improvements in the performance as well since quantum algorithms operate on logarithmically smaller number of memory units compared to classical algorithms. Finding such efficient quantum algorithms for domain-specific applications is a key objective of quantum simulation research.

Previous works presented quantum algorithms for calculating the electromagnetic scattering cross section [31], performing quantum beam propagation in homogeneous media [32], and simulating quantum optical systems [33]. In this work, we simulate wave optics on quantum computers by solving the Helmholtz equation for a scalar field in a medium with a slowly varying refractive index. The simulator is implemented using an efficient and flexible block-encoding structure that can be tuned to simulate the effects of various optical elements on an incident light beam. The implementation uses an ancillary quantum register to construct block-encoded phase shifters acting on a target register. Using a split-step technique [34], these phase shifters are used along with quantum Fourier transformation (QFT) subroutines [35] to simulate wave propagation in the paraxial approximation. The ancillary register only needs

\* siavash.davani@uni-jena.de

† martin.gaerttner@uni-jena.de

‡ falk.eilenberger@uni-jena.de

$\log_2 N$  number of qubits, and the gate complexity of the simulator is quadratic in the simulation time  $\mathcal{O}(t^2)$ . Therefore, this algorithm establishes a significant improvement in computational capacity for high-precision applications.

Section II discusses the reduction of the Helmholtz equation to a time-dependent Hamiltonian simulation problem. In Section III, the block-encoding of phase propagators is introduced and its relation to Hamiltonian simulations is discussed. And Section IV presents the simulation of a Gaussian beam incident on a plano-convex lens using the phase propagators.

## II. PRELIMINARIES

### A. Fresnel-approximated wave optics in weakly inhomogeneous media as a Hamiltonian simulation problem

The scalar wave equation for a field  $u(\mathbf{r}, \omega)$  propagating in a weakly inhomogeneous medium is

$$\Delta u(\mathbf{r}, \omega) + k^2(\mathbf{r}, \omega)u(\mathbf{r}, \omega) = 0, \quad (1)$$

known as the Helmholtz equation [36], where

$$k^2(\mathbf{r}, \omega) = \frac{\omega^2}{c^2} \epsilon(\mathbf{r}, \omega) \quad (2)$$

is the wave number squared; and  $\omega$ ,  $\epsilon$ ,  $c$ , and  $\Delta$  are, respectively, the angular frequency of the monochromatic wave, relative permittivity of the medium, light velocity in vacuum, and Laplacian operator. Eq. (1) describes the propagation of a wave in an isotropic, dispersive, and inhomogeneous material as long as  $\epsilon(\mathbf{r}, \omega)$  varies slowly as a function of the spatial coordinate  $\mathbf{r}$ , that is to say

$$\left| \frac{\nabla \epsilon(\mathbf{r}, \omega)}{\epsilon(\mathbf{r}, \omega)} \right| \ll \frac{1}{\lambda}. \quad (3)$$

In our discussion, we consider the case of a monochromatic wave and leave out the  $\omega$  dependency of  $\epsilon$  from now on. We also assume that the radiation is localized in the momentum space and apply the paraxial approximation. Without loss of generality, we choose the  $z$  coordinate axis to align with the optical axis. After these assumptions, the solution to Eq. (1) takes the form of

$$u(\mathbf{r}) = v(\mathbf{r})e^{i\tilde{k}z}, \quad (4)$$

where  $\tilde{k} = \langle k(\mathbf{r}) \rangle$  is the wavenumber averaged over the volume of the simulation space. Putting this ansatz in Eq. (1) leads to the following differential equation for  $v(\mathbf{r})$

$$i \frac{\partial}{\partial z} v(\mathbf{r}) + \frac{1}{2\tilde{k}} \Delta_{x,y} v(\mathbf{r}) + \frac{k^2(\mathbf{r}) - \tilde{k}^2}{2\tilde{k}} v(\mathbf{r}) = 0, \quad (5)$$

where  $\Delta_{x,y} = \frac{\partial^2}{\partial x^2} + \frac{\partial^2}{\partial y^2}$  is the transverse Laplacian operator. Since we chose the  $z$  axis to match the direction of propagation, we can separate the transverse coordinates  $\mathbf{r}_\perp = x\mathbf{e}_x + y\mathbf{e}_y$  and the propagation coordinate  $z = ct$  to rewrite the differential equation as

$$i \frac{1}{c} \frac{\partial}{\partial t} v(t; \mathbf{r}_\perp) + \frac{1}{2\tilde{k}} \Delta_{x,y} v(t; \mathbf{r}_\perp) + \frac{k^2(t; \mathbf{r}_\perp) - \tilde{k}^2}{2\tilde{k}} v(t; \mathbf{r}_\perp) = 0. \quad (6)$$

This equation is a first-order differential equation in time and resembles the form of the Schrödinger equation

$$i\hbar \frac{\partial}{\partial t} |v(t)\rangle = \hat{H}(t) |v(t)\rangle, \quad (7)$$

where

$$\langle \mathbf{r}_\perp | v(t) \rangle = v(t; \mathbf{r}_\perp), \quad (8)$$

and the Hamiltonian of the system is

$$\hat{H}(t) = \frac{c}{2\hbar\tilde{k}} (\hat{p}_x^2 + \hat{p}_y^2) - \frac{\hbar c}{2\tilde{k}} (k^2(t; \hat{x}, \hat{y}) - \tilde{k}^2) \quad (9)$$

$$= T(\hat{p}_x, \hat{p}_y) + V(t; \hat{x}, \hat{y}), \quad (10)$$

where  $T$  and  $V$  are the kinetic and potential terms. This shows that the problem of beam propagation in weakly inhomogeneous media reduces to a time-dependent Hamiltonian simulation problem and hence can be solved using a quantum computer. Note that the potential energy term in the Hamiltonian is time-dependent (or equivalently  $z$ -dependent in this case) because the propagating beam interacts with a varying refractive index during the propagation.

A simulation algorithm starts with a field distribution in the transverse plane  $|v(t_i)\rangle$  at an initial time  $t_i$  and evolves the field after propagating for time  $t$  or distance  $\Delta z = ct$  in the direction of propagation to compute  $|v(t_i + t)\rangle$ . The time dependency of the Hamiltonian and non-commuting kinetic and potential energy terms in Eq. (10) make this computation non-trivial. We use a split-step method [34] to perform the computation on a quantum computer by dividing the evolution time into a discrete number of small time steps and execute the corresponding unitary steps sequentially.

Let us partition the total evolution time from  $t_i = 0$  to  $t_f = t$  into  $r$  equal intervals  $\Delta t = t/r$  and pick arbitrary times  $t_j$  as representatives of their corresponding partition  $t_j \in [j\Delta t, (j+1)\Delta t]$  where  $j = 0, 1, \dots, r-1$ . Assuming  $\Delta t$  is small and using the first-order Trotter-Suzuki formula [37], we can approximate the total time evolution operator (setting  $\hbar = 1$ ) as

$$\hat{U}(t, 0) = \prod_{j=0}^{r-1} e^{-i\hat{T}\Delta t} e^{-i\hat{V}(t_j)\Delta t} + \mathcal{O}(\Delta t^2). \quad (11)$$

This means, to execute the time evolution, we need to sequentially apply unitary propagation steps of the form  $e^{-i\hat{T}\Delta t}$  and  $e^{-i\hat{V}\Delta t}$  to the initial state  $|v(0)\rangle$ . In Section III, we construct block-encoded operators that implement such unitary steps and use them to realize  $\hat{U}(t, 0)$ .

It is also worth mentioning that we have used the first-order Trotter formula in this discussion because of its simplicity. However, it is potentially possible to use more advanced methods such as higher-order Trotterization [38] or Dyson series [39] to achieve a more favorable scaling of the time discretization error with  $\Delta t$ . However, our main objective in this work is to implement evolution operators for a small step size using block-encoding, which then can also be used in other time discretization schemes.

## B. Block-encoding

Before presenting the main results we briefly review the notion of block-encoding. Block-encoding is an intuitive and useful way to model non-unitary operations on quantum computers. The formal definition of block-encoding is given in the following. The presentation follows [21].

**Definition 1 (Block-encoding)** *A unitary operator  $U_A$  is called an  $(\alpha, a, \epsilon)$ -block-encoding of the (not necessarily unitary) operator  $A$  if*

$$\left\| A - \alpha \left( \langle 0|^{\otimes a} \otimes I \right) U_A \left( |0\rangle^{\otimes a} \otimes I \right) \right\| \leq \epsilon \quad (12)$$

As an intuitive example to the above definition, an exact block-encoding of  $A$  ( $\epsilon = 0$ ) takes the form of

$$U_A = \begin{pmatrix} A/\alpha & * \\ * & * \end{pmatrix}, \quad (13)$$

meaning that  $A$  occupies the top left block of  $U_A$ , and  $*$  indicates that the exact values of the other blocks of  $U_A$  are not important as long as  $U_A$  is a unitary operator. If  $A$  was unitary and we knew how to construct it on a quantum computer, we could directly apply it to a register  $|\psi\rangle$  to achieve the result

$$A|\psi\rangle. \quad (14)$$

But since  $A$  can be non-unitary,  $A|\psi\rangle$  is not necessarily normalized thus we can only hope having probabilistic access to it. The block-encoding  $U_A$  provides such probabilistic access. In this example, an  $a$ -qubit ancillary register is added to the primary register to form  $|0\rangle^{\otimes a} |\psi\rangle$  and the block-encoding  $U_A$  acts on the combined register

$$U_A |0\rangle^{\otimes a} |\psi\rangle = |0\rangle^{\otimes a} \frac{A|\psi\rangle}{\alpha} + |\perp\rangle, \quad (15)$$

where  $\langle\langle 0|^{\otimes a} \otimes I | \perp \rangle\rangle = 0$ . If we post-select the  $a$ -qubit ancillary register being in the zero state, the primary register is projected into a state proportional to  $A|\psi\rangle$ , meaning that the ancillary register flags the success case. The probability of success of the post-selection is

$$P_{\text{success}} = \frac{1}{|\alpha|^2} \langle\psi| A^\dagger A |\psi\rangle. \quad (16)$$

Note that any unitary operator is trivially a  $(1, 0, 0)$ -block-encoding of itself; hence using the block-encoding framework, we can extend the analysis of quantum algorithms beyond unitary operations by allowing for ancillary registers, probabilistic success, and flagging of the success case.

### III. RESULTS

In order to implement the time evolution operator in Eq. (11), we first construct a block-encoding of a generic phase operator

$$e^{i \sum_x \Delta |\phi(x)|^2 |x\rangle\langle x|} \quad (17)$$

for a small coefficient  $\Delta$  and a normalized wavefunction  $\phi(x)$ . This operator applies the phase  $e^{i\Delta|\phi(x)|^2}$  to the register it acts on. Because the unitary propagators  $e^{-i\hat{V}\Delta t}$  and  $e^{-i\hat{T}\Delta t}$  from Eq. (11) are diagonal phase operators in position and momentum basis respectively, the block-encoding unit in Eq. (17) implements those propagators in their corresponding basis by choosing relevant  $\Delta$  and  $\phi(x)$  parameters. Hence, the block-encoding unit realizes a single time step of the unitary evolution for a small step size, and this unit is then used in iterations to simulate arbitrarily long dynamics. The circuit representation of the block-encoding unit is presented in Fig. 1,

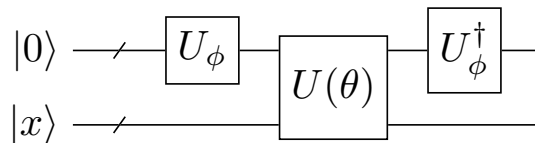


FIG. 1: The schematic circuit representation of the block-encoding unit for the phase protocol.

where  $U_\phi$  is an amplitude oracle unitary that prepares the state  $|\phi\rangle$  in the  $n$ -qubit ancillary register

$$U_\phi |0\rangle = |\phi\rangle = \sum_{x=0}^{2^n-1} \phi(x) |x\rangle, \quad (18)$$

and  $U(\theta)$  is defined as a conditional phase shifter

$$U(\theta) |y\rangle |x\rangle = \begin{cases} e^{i\theta} |y\rangle |x\rangle, & \text{for } x = y \\ |y\rangle |x\rangle, & \text{for } x \neq y \end{cases}. \quad (19)$$

The block-encoding consumes the ancillary state  $|\phi\rangle$  to apply the  $e^{i\Delta|\phi(x)|^2}$  phase to the  $n$ -qubit primary register  $|x\rangle$ . We assume the existence of an efficient initializer for the desired  $|\phi\rangle$  state and acknowledge that constructing initializers for a given state is not always trivial and is currently a topic of active research. If the phase profile is a smooth signal with a bounded first derivative, one can use techniques based on matrix product states [40, 41] to prepare the state efficiently. For an overview of the state preparation problem and the representation of data on a quantum computer see [5, 42].

The role of the  $U(\theta)$  operator is to establish the necessary entanglement between the registers to achieve the desired phase transformation at the end. This operator is efficiently implemented using  $\mathcal{O}(n)$  number of elementary gates. The general implementation of the operator in the case of arbitrary  $n$  is discussed in Appendix A. However, as an example, the implementation for  $n = 3$  is presented in Fig. 2, where  $P(\theta) = \begin{bmatrix} 1 & 0 \\ 0 & e^{i\theta} \end{bmatrix}$  is the elementary phase operator.

The efficient  $\mathcal{O}(n)$  gate complexity means that, in most cases, the  $U(\theta)$  operator will not be the limiting factor in the performance of the protocol considering the usually higher gate complexity of the state preparation unitary  $U_\phi$ .

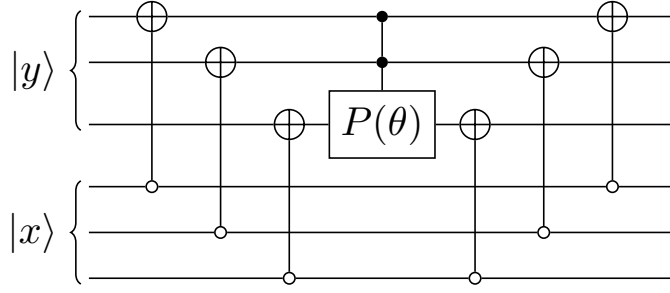


FIG. 2: The implementation of the conditional phase operator  $U(\theta)$  in the case of 3-qubit input registers using CNOT gates and a controlled phase gate.

Also, when the protocol is used together with the quantum Fourier transformation (QFT), e.g. in most simulation problems, the performance will be limited by the higher  $\mathcal{O}(n^2)$  gate complexity of QFT.

Direct calculation (Appendix B) of the output of the circuit in Fig. 1 shows that the circuit is a  $(1, n, 0)$ -block-encoding of the operator

$$A(\theta) = I + 2ie^{i\frac{\theta}{2}} \sin \frac{\theta}{2} \sum_x |\phi(x)|^2 |x\rangle\langle x| \quad (20)$$

such that the following transformation is performed by the circuit

$$U_A |0\rangle^{\otimes n} |\psi\rangle = |0\rangle^{\otimes n} A(\theta) |\psi\rangle + |\perp\rangle, \quad (21)$$

the success probability of the operation (namely the probability of the ancillary register being  $|0\rangle$ ) is

$$\begin{aligned} P_{\text{success}} &= \langle \psi | A^\dagger(\theta) A(\theta) | \psi \rangle \\ &\geq 1 - \sin^2 \frac{\theta}{2}. \end{aligned} \quad (22)$$

If we take the angle of the conditional rotation to be small  $\theta = \Delta \ll 1$ , in the first order approximation in  $\Delta$ , we apply the operator

$$\begin{aligned} A(\Delta) &= I + i\Delta \sum_x |\phi(x)|^2 |x\rangle\langle x| + \mathcal{O}(\Delta^2) \\ &= e^{i\Delta \sum_x |\phi(x)|^2 |x\rangle\langle x|} + \mathcal{O}(\Delta^2) \end{aligned} \quad (23)$$

to the state in the primary register with the success probability of

$$P_{\text{success}} = 1 - \mathcal{O}(\Delta^2). \quad (24)$$

Starting with the primary register in the state  $|\psi\rangle = \sum_x \psi(x) |x\rangle$ , we effectively apply a phase to this state as

$$|\psi\rangle = \sum_x \psi(x) |x\rangle \longrightarrow |\psi'\rangle \approx \sum_x \psi(x) e^{i\Delta |\phi(x)|^2} |x\rangle \quad (25)$$

with arbitrarily high probability. The circuit in Fig. 1 is thus a  $(1, n, \mathcal{O}(\Delta^2))$ -block-encoding of the operator

$$e^{i\Delta \sum_x |\phi(x)|^2 |x\rangle\langle x|}. \quad (26)$$

This means if we post-select the success case and repeatedly apply the circuit  $m$  times, we will effectively implement the operator

$$e^{i \sum_x \alpha |\phi(x)|^2 |x\rangle\langle x|}, \quad (27)$$

where  $\alpha = m\Delta$  and error of this implementation is  $\epsilon = \mathcal{O}(m\Delta^2) = \mathcal{O}(\frac{\alpha^2}{m})$ .

Comparing this result to the potential and kinetic propagators we needed for the simulation in Eq. (11), namely

$$e^{-iV(\hat{x})\Delta t} = e^{-i\sum_x V(x)\Delta t|x\rangle\langle x|} \quad (28)$$

and

$$e^{-iT(\hat{p})\Delta t} = e^{-i\sum_p T(p)\Delta t|p\rangle\langle p|}, \quad (29)$$

reveals that we can simulate the time evolution by choosing suitable ancillary states  $|\phi\rangle$  and phase coefficients  $\alpha$  corresponding to the desired phase profiles  $V(x)\Delta t$  and  $T(p)\Delta t$  and respectively apply the phase transformations to the primary register  $|\psi\rangle$  in the real and Fourier domains. Applying the phase in the Fourier domain additionally involves using quantum Fourier transformation on the primary register. This analysis shows that in order to perform a time evolution for total time  $t$  with a maximum tolerated error  $\epsilon$ , we need  $m = \mathcal{O}(\frac{t^2}{\epsilon})$  number of iterations. Also note that the block-encoding in Eq. (23) directly implements the first-order Taylor expansion of the unitary

$$e^{i\sum_x \Delta|\phi(x)|^2|x\rangle\langle x|} \quad (30)$$

therefore does not need further quantum signal processing [21, 43]. The requirement of the protocol on the  $\Delta$  parameter to be small also fits well with the assumption of small  $\Delta t$  in the Trotter scheme used to simplify the total time evolution unitary in Eq. (11).

#### IV. SIMULATIONS

To showcase the algorithm, we simulated the propagation of a one-dimensional Gaussian beam in a 2-dimensional setup passing through a spherical (plano-convex) lens. We assume the paraxial approximation and align the  $z$  axis to the propagation direction. The lens is expected to cause the beam to focus at a certain propagation distance after the lens. The lens has a finite non-zero thickness, and due to the spherical shape of its surface, spherical aberrations are expected to appear. The lens is also assumed to be lossless, therefore it only imprints phases on the incident beam. The schematic plot of the setup is shown in Fig. 3.

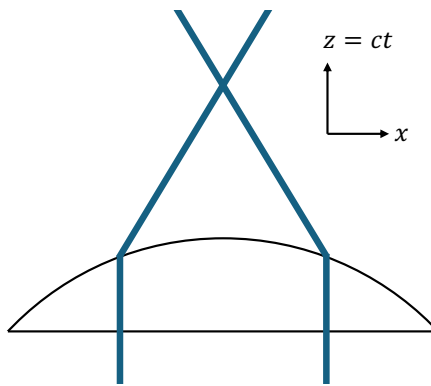


FIG. 3: Schematic figure of the simulation setup. The beam is propagating in the  $z$  direction.

Following the split-stepping procedure described in Eq. (11), in order to perform the simulation using the protocol, we cut the lens in the propagation axis and approximate it as a stack of thin rectangular layers of material. This procedure is shown in Fig. 4. Note that the propagation distance  $z$  and the elapsed time are interchangeable according to  $z = ct$ .

This allows us to propagate the beam through the lens step-by-step by sequentially applying a rectangular phase profile to the field (in the real domain) and propagating it for the thickness of each layer (quadratic phase profile in the Fourier domain). For the phase corresponding to each layer of material in real domain, the ancillary state  $|\phi\rangle$  is chosen as a rectangular state where its width is calculated using the curvature of the lens' surface and the phase coefficient  $\alpha$  is chosen such that the part of the field passing through the material picks up a phase equal to  $\Delta\theta = (n - 1)k_0l$ , where  $n$ ,  $k_0$ , and  $l$  are respectively the refractive index of the material, wavenumber in vacuum, and thickness of each slice (Fig. 5).

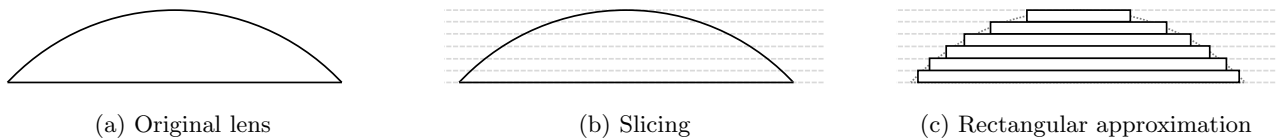


FIG. 4: Slicing the lens and approximating it by a stack of rectangular layers with a fixed thickness in the propagation direction.

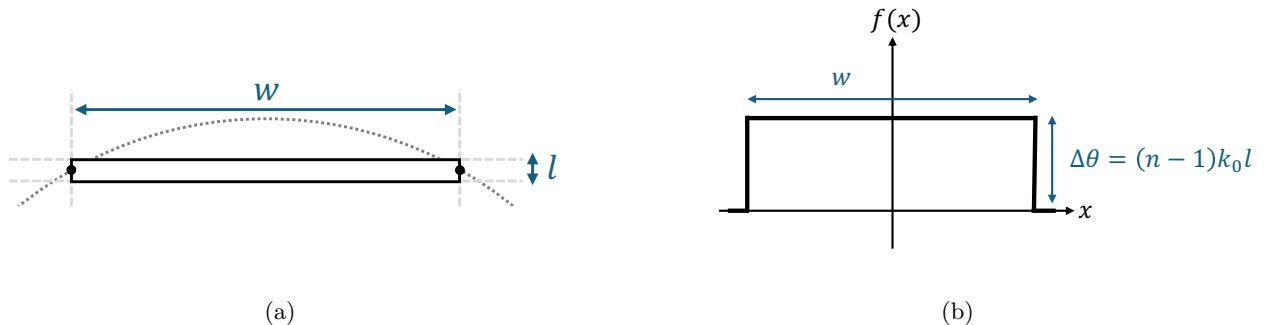


FIG. 5: The phase difference that each layer of the material imprints on the incident beam depending on whether the corresponding part of the wave in the transverse axis passes through the material or propagates through the vacuum outside the material. (a) The geometry of a slice of the lens. (b) The corresponding relative phase  $e^{if(x)}$  each slice of the lens imprints on the incident beam in the real domain.

This specific approximation is not unique nor necessarily the most accurate and is chosen here for its simplicity. We note that the ability of the phase protocol to tune the applied phase profiles provides great flexibility to design and explore various possibilities for such simulations.

Moreover, the kinetic energy part of the Hamiltonian that simulates the propagation of the field in the  $z$  axis is implemented in three steps: (1) applying a quantum Fourier transformation on the state  $|\psi\rangle$ , (2) applying the paraxial-approximated transfer function (a quadratic phase) to the Fourier transform of the field as

$$H_f(k) = e^{-i\frac{k^2}{2k_0}z}, \quad (31)$$

where  $z$  is the propagation distance, and finally (3) applying an inverse QFT to retrieve the propagated field in the real domain.

We ran the simulation for the wavelength, initial Gaussian beam waist, refractive index, radius of curvature, and number of qubits, respectively being  $\lambda = 1\mu m$ ,  $w_0 = 25\mu m$ ,  $n = 1.25$ ,  $R = 50\mu m$ , and  $n_q = 7$ . The result of this simulation is presented in Fig. 6.

Summarizing our observation from Fig. 6, firstly, our results reproduce the expected focusing of the beam. Furthermore, we see the interference of out of phase refracted components of the wave before reaching the focus which is an aberration expected from a thick lens with a spherical surface. However, it is also known that these aberration effects will decrease if we change the orientation of the lens such that the incident beam hits the convex surface first. To showcase the flexibility of this simulation protocol, we performed the simulation in the reverse orientation and several other cases, such as lenses with parabolic surface curvature, and the results are presented in Appendix C.

Next, we characterized the performance of the quantum simulation. The most important parameter in the performance is the maximum allowed phase coefficient  $\Delta_{max}$  in the block-encodings, which is the source of error in the phase shifters in Eq. (23). For benchmarking the effect of  $\Delta_{max}$ , we ran simulations keeping all the simulation parameters fixed except for  $\Delta_{max}$  which was chosen from  $[0.001, 0.2]$  and analyzed two metrics: accuracy and probability of success. The expectation is that decreasing  $\Delta_{max}$  leads to higher accuracy and also higher probability of success at the cost of more simulation steps, i.e. larger gate count and simulation time.

For measuring the accuracy, we calculated the fidelity between the output state of the quantum simulation and the state resulting from classical calculations at a fixed propagation distance  $z \approx 200\mu m$ . The classical simulation was done by directly multiplying the incident light field by the corresponding phases from the simulation scheme in Eq. (11) and using classical discrete Fourier transformation for kinetic energy terms. With that, we isolated the effects of the errors explicitly resulting from the block-encoded phase operators of the quantum simulation protocol. The result is shown in Fig. 7a.

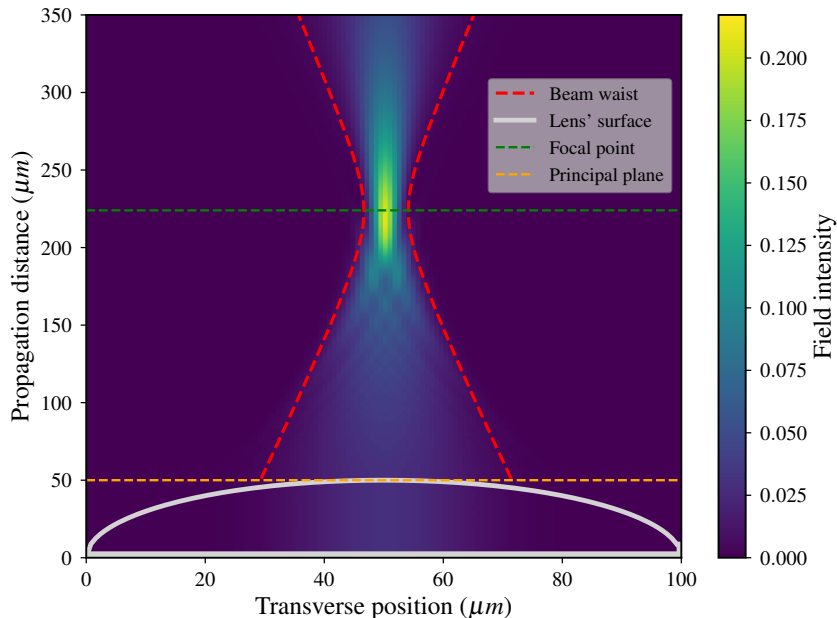


FIG. 6: The result of the quantum simulation of a Gaussian beam incident on a plano-convex lens. For this simulation, the maximum delta was  $\Delta_{max} = 0.01$  and the lens was sliced into 10000 layers.

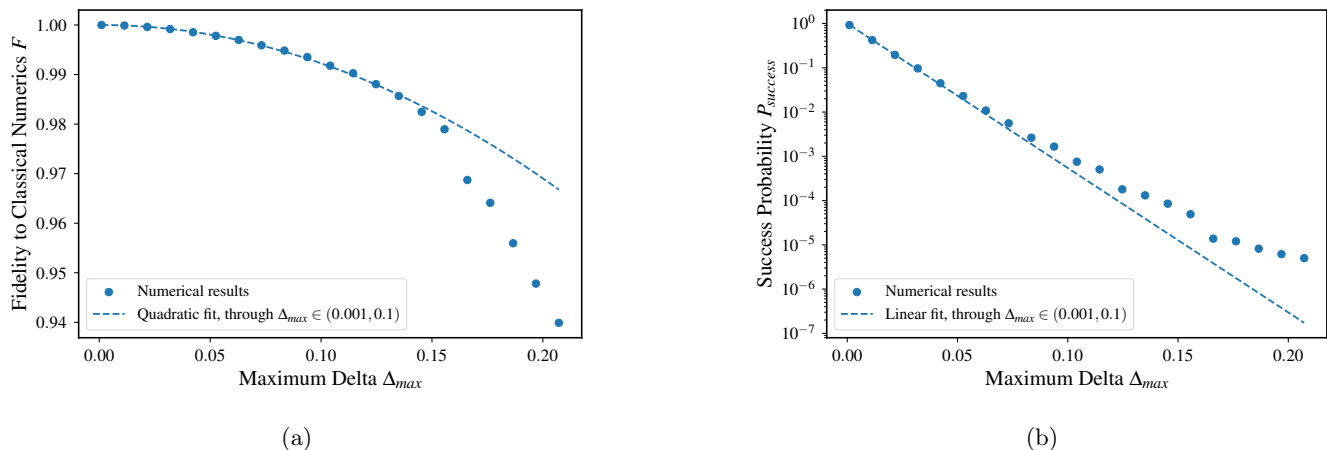


FIG. 7: Characterization of the error and the performance of the quantum simulation. (a) The fidelity between the resulting wavefunction from the quantum simulation and the classical numerical result by directly multiplying the field with the phases (calculated at  $z \approx 200\mu m$ ), post-selecting successful outcomes. (b) The probability of success of the quantum simulation, that is the probability of all post-selections leading to the desired outcome. In these simulations, the number of qubits was  $n_q = 6$ .

From analytical calculations (Appendix B), assuming the total number of uses of the block-encoding is  $M = \mathcal{O}(1/\Delta_{max})$  for sufficiently small  $\Delta_{max}$ , we expect the fidelity as a function of  $\Delta_{max}$  to behave as

$$F = 1 - \mathcal{O}(\Delta_{max}^2) \quad (32)$$

and this is confirmed by fitting a quadratic function to the fidelity in Fig. 7a for small values of  $\Delta_{max}$ . Note that the fidelities are calculated in the case of successful post-selections. To fully characterize the simulation protocol, we should also analyze the success probability. The total probability of success as a function of small  $\Delta_{max}$  is

$$P_{success} = 1 - \mathcal{O}(\Delta_{max}). \quad (33)$$

meaning that for small  $\Delta_{max}$  we expect a linear behavior which is seen in Fig. 7b. We conclude the discussion by mentioning that, although it is not straightforward to calculate an exact practical value for  $\Delta_{max}$  to achieve high accuracy for a particular simulation problem, it can be said that as long as the probability of success is high, i.e. post-selections are successful, we can be sure that the accuracy will also be high. This makes the success or failure of the post-selection process a measure for the accuracy of the simulation as well. In a real-world application, one can start with a reasonable value of  $\Delta_{max}$  and adapt by tuning it to smaller values if a simulation trial fails.

## V. CONCLUSION

In this work, we discussed how the problem of wave propagation in a weakly inhomogeneous medium in the paraxial approximation is reduced to a time-dependent Hamiltonian simulation problem. We then introduced a block-encoding that enables unitary time evolutions accurate to the first-order approximation in time. The method is highly flexible since the Hamiltonian to be simulated is programmed in the quantum computer using an amplitude oracle. This tunability allows for the simulation of optical elements with various refractive index distributions, as long as the corresponding phase profiles can be encoded in a quantum register. The algorithm is exponentially efficient in memory consumption, requiring  $\mathcal{O}(\log N)$  number of qubits for a discretized light field with the grid size of  $N$  in the transverse plane. And a similar improvement for the circuit depth is possible for simulations involving refractive index distributions that are efficiently preparable in quantum registers. This efficiency promises quantum advantage for a range of high-precision applications. We also showcased the algorithm by numerically simulating a simple wave optics experiment. There is a tradeoff between the time discretization step size  $\Delta_{max}$  and the accuracy of the simulation such that keeping  $\Delta_{max}$  small leads to lower simulation errors at the expense of deeper quantum circuits.

It must be pointed out that the simulation protocol described in this work will not be efficient if the objective is to extract the complete propagated field for a given propagation distance, because the output is computed as wavefunction amplitudes in a quantum register. Trying to extract the field intensity from this quantum register by direct measurement will inevitably lead to losing the quantum efficiency. State tomography to extract the field will also have the same effect. Instead, one has to choose a particular observable and only extract information about that using techniques such as the Hadamard test [5]. This is, however, not a drawback particular to this protocol but a general consideration for many quantum numerical solvers. Nevertheless, focusing on one observable can still be very beneficial, for example, in an optical design application where the observable can be the coupling efficiency, mode overlap, or a particular Zernike coefficient which needs to be minimized or maximized for a particular application. The ability to efficiently simulate the propagation of a light field through optical elements allows for rapidly iterating over and optimizing the design of optical systems, and a performant quantum simulator that estimates design loss functions can greatly enhance iterative design processes.

While the simulation algorithm introduced here, in its current form, is limited to small numerical apertures and cannot yet treat polarization, it shows not only that quantum-enabled optical systems design is feasible, but also that exponential speedup is a possibility. We expect our work to motivate the optics community to consider quantum computing as a promising platform for optical simulation and to further investigate the utility of recent developments in quantum algorithms such as block-encoding and quantum signal processing for advances in the field.

## ACKNOWLEDGMENTS

This research is funded by the Deutsche Forschungsgemeinschaft (DFG, German Research Foundation) – Project-ID 398816777 – SFB 1375. F.E. and S.D. are affiliated with the Max Planck School of Photonics supported by the German Federal Ministry of Education and Research (BMBF), the Max Planck Society and the Fraunhofer Society.

## AUTHOR CONTRIBUTIONS

All authors contributed equally to the scientific content of this work. S.D. was a major contributor to developing the simulation codes. All authors read and approved the final manuscript.

## DATA AND SOURCE CODE AVAILABILITY

The source code is publicly available in a git repository at <https://github.com/BlackWild/qiu>. Snapshots of the repository and the datasets generated and analyzed in this work are permanently stored at <https://doi.org/10.>

5281/zenodo.19333735 and <https://doi.org/10.5281/zenodo.19333783> respectively.

**COMPETING INTERESTS**

All authors declare that they do not have any known financial or non-financial competing interests regarding this work.

**Appendix A: The implementation of the partial phase operator**

Here, we provide the details of the implementation of the  $U(\Delta)$  operator introduced in Section III. The implementation needs  $\mathcal{O}(n)$  gates where  $n$  is the number of qubits of each of the input registers.

The operator is defined in terms of its action on the computational basis states as

$$U(\Delta) |y\rangle |x\rangle = \begin{cases} e^{i\Delta} |y\rangle |x\rangle, & \text{for } x = y \\ |y\rangle |x\rangle, & \text{for } x \neq y \end{cases} \tag{A1}$$

The goal is to implement this operator by decomposing it into elementary single- and two-qubit gates. The key to its implementation is that the condition  $x = y$  in Eq. (A1) is realized when all corresponding qubits of the registers  $|x\rangle$  and  $|y\rangle$  are in the same state. If we represent the basis states of each register as the tensor product of the underlying qubits, we have

$$|x\rangle = |x_{n-1}\rangle \cdots |x_1\rangle |x_0\rangle, \tag{A2}$$

and similarly

$$|y\rangle = |y_{n-1}\rangle \cdots |y_1\rangle |y_0\rangle, \tag{A3}$$

where  $x_j \in \{0, 1\}$  and  $y_j \in \{0, 1\}$  are the binary digits of the binary representations of  $x$  and  $y$ . The condition  $x = y$  is equivalent to  $x_j = y_j$  for all  $j$ .

The equality of each qubit pair can be checked via elementary unitary operations. To check the condition  $x_j = y_j$  we should calculate the flag bit  $z_j = y_j \oplus \overline{x_j}$ , where  $\oplus$  is the XOR logical operator and the overline in  $\overline{x_j}$  represents the logical NOT operation. The flag state  $|z_j\rangle = |y_j \oplus \overline{x_j}\rangle$  can thus be computed using a CNOT gate acting on the  $|y_j\rangle$  qubit with the control qubit of  $|x_j\rangle$  and control state of 0.

$$CNOT_0 |x_j\rangle |y_j\rangle = |x_j\rangle |y_j \oplus \overline{x_j}\rangle = |x_j\rangle |z_j\rangle \tag{A4}$$

Using  $n$   $CNOT_0$  gates, we can compute all the flag bits  $z_j$  and then a multi-controlled phase gate  $P(\Delta)$  with the phase parameter  $\Delta$  acting on the  $|z_j\rangle$  qubits will apply the phase to the state if all the  $|z_j\rangle$  qubits are  $|1\rangle$  which is equivalent to the condition  $x = y$ . And finally, the temporarily computed  $|z_j\rangle$  states are uncomputed by applying the same CNOT gates again.

As an example, the implementation for the case of 3-qubit quantum registers ( $n = 3$ ) is presented in Fig. 8. Despite the appearance of the circuit structure, the  $U(\Delta)$  operator is in fact symmetric with respect to the exchange of its input registers, as it is clear from Eq. (A1).

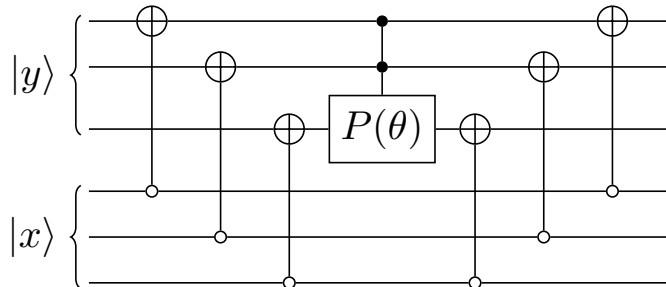


FIG. 8: The implementation of the partial phase operator  $U(\Delta)$  in the case of 3-qubit input registers.

As we see in this implementation, we need  $2n$  CNOT gates and one multi-controlled phase gate acting on  $n$  qubits. Because the multi-controlled phase gate can be implemented using  $\mathcal{O}(n)$  gates [35], the total gate complexity of the  $U(\Delta)$  operator is  $\mathcal{O}(n)$ .

## Appendix B: Derivation of the block-encoding

Here, we provide the derivation details of the results discussed in Section III about the block-encoding of

$$A(\theta) = I + 2i e^{i\frac{\theta}{2}} \sin\left(\frac{\theta}{2}\right) \sum_x |\phi(x)|^2 P_x, \quad (\text{B1})$$

and that in the approximation  $\theta = \Delta \ll 1$ , we have

$$A(\Delta) \approx e^{i\Delta \sum_x |\phi(x)|^2 |x\rangle\langle x|}. \quad (\text{B2})$$

Let us start by finding a useful representation of the partial phase operator. The operator that was defined in Eq. (A1) can be rewritten as

$$U(\theta) = \sum_x \left( \left[ e^{i\theta} P_x + \sum_{y \neq x} P_y \right] \otimes P_x \right), \quad (\text{B3})$$

where  $P_x = |x\rangle\langle x|$  is the projection operator that projects vectors to the  $|x\rangle$  basis state. Using the completeness relation  $\sum_y P_y = I$ , we have

$$U(\theta) = \sum_x \left[ I + 2i e^{i\frac{\theta}{2}} \sin\left(\frac{\theta}{2}\right) P_x \right] \otimes P_x \quad (\text{B4})$$

$$= I \otimes I + 2i e^{i\frac{\theta}{2}} \sin\left(\frac{\theta}{2}\right) \sum_x P_x \otimes P_x. \quad (\text{B5})$$

In the form represented in Eq. (B5), it is easy to see how the operator gets close to the identity  $I \otimes I$  when  $\theta$  tends to zero. To simplify the notation for the following derivations, we define  $U_x = I + 2i e^{i\frac{\theta}{2}} \sin\left(\frac{\theta}{2}\right) P_x$  and rewrite Eq. (B4) as

$$U(\theta) = \sum_x U_x \otimes P_x. \quad (\text{B6})$$

This operator still does not contain any reference to the  $\phi(x)$  state and is not the block-encoding of  $A(\theta)$  from Eq. (B1), and because of that, it does not have the tunability to apply  $x$ -dependent phase profiles. We need to include the  $U_\phi$  operators to form the complete block-encoding.  $U_\phi$  is defined such that it prepares the  $|\phi\rangle$  state acting on the zero state  $|\phi\rangle = U_\phi |0\rangle$ . Let us now construct the complete block-encoding unitary  $U$  including the  $U_\phi$  and  $U_\phi^\dagger$  operators acting on the ancillary register

$$\begin{aligned} U &= \left( U_\phi^\dagger \otimes I \right) \left( U(\theta) \right) \left( U_\phi \otimes I \right) \\ &= \sum_x U_\phi^\dagger U_x U_\phi \otimes P_x. \end{aligned} \quad (\text{B7})$$

This means that the unitary  $U$  is a block-encoding of the following operator

$$A(\theta) = \left( \langle 0| \otimes I \right) U \left( |0\rangle \otimes I \right) \quad (\text{B8})$$

$$= \sum_x \left( \langle 0| U_\phi^\dagger U_x U_\phi |0\rangle \right) P_x \quad (\text{B9})$$

$$= \sum_x \left( 1 + 2i e^{i\frac{\theta}{2}} \sin\left(\frac{\theta}{2}\right) |\phi(x)|^2 \right) P_x \quad (\text{B10})$$

$$= I + 2i e^{i\frac{\theta}{2}} \sin\left(\frac{\theta}{2}\right) \sum_x |\phi(x)|^2 P_x, \quad (\text{B11})$$

which is equal to the operator we wanted to construct (Eq. (B1)).

The probability of success of the post selection, assuming the primary state was initially  $|\psi\rangle = \sum \psi(x) |x\rangle$ , is

$$P_{\text{success}} = \langle \psi | A(\theta)^\dagger A(\theta) | \psi \rangle = \sum_x |\psi(x)|^2 \left( 1 - 4 \sin^2\left(\frac{\theta}{2}\right) |\phi(x)|^2 (1 - |\phi(x)|^2) \right) \quad (\text{B12})$$

$$\geq 1 - \sin^2 \frac{\theta}{2}. \quad (\text{B13})$$

And the wavefunction after post-selection is

$$|\psi'\rangle = \frac{A(\theta) |\psi\rangle}{\sqrt{P_{\text{success}}}}. \quad (\text{B14})$$

This proves the main result in Eq. (B1) and the case of  $\theta = \Delta \ll 1$  is discussed in the main text in Section III.

And finally, we calculated the asymptotic behavior of the fidelity between the ideal output and the approximate result from the block-encoding in the general case of  $m$  successful iterations while keeping the total applied phase coefficient  $\alpha = m\Delta$  fixed. Namely  $F = |O|^2$ , where

$$O = \langle \psi | e^{-i\alpha|\phi(\hat{x})|^2} \frac{A^m(\Delta)}{\sqrt{P_{\text{success}}^m}} | \psi \rangle \quad (\text{B15})$$

$$= \sum_x |\psi(x)|^2 \left[ e^{-i\alpha|\phi(x)|^2} \right] \left[ 1 + 2i e^{i\frac{\alpha}{2m}} \sin\left(\frac{\alpha}{2m}\right) |\phi(x)|^2 \right]^m \left[ \frac{1}{\sqrt{1 - 4C^2 \sin^2 \frac{\alpha}{2m}}} \right]^m, \quad (\text{B16})$$

where  $C^2 = \sum_x |\psi(x)|^2 |\phi(x)|^2 (1 - |\phi(x)|^2)$ . Performing a Taylor series expansion of  $O$  in Eq. (B16) at  $m = \infty$  leads to the result of

$$F = 1 - \mathcal{O}\left(\frac{\alpha^4}{m^2}\right) = 1 - \mathcal{O}(\alpha^2 \Delta^2). \quad (\text{B17})$$

Furthermore, the total probability of success of  $m$  post-selections is

$$P_{\text{success}} = \left[ \sqrt{1 - 4C^2 \sin^2 \frac{\alpha}{2m}} \right]^{2m} = 1 - \mathcal{O}\left(\frac{\alpha^2}{m}\right) = 1 - \mathcal{O}(\alpha \Delta). \quad (\text{B18})$$

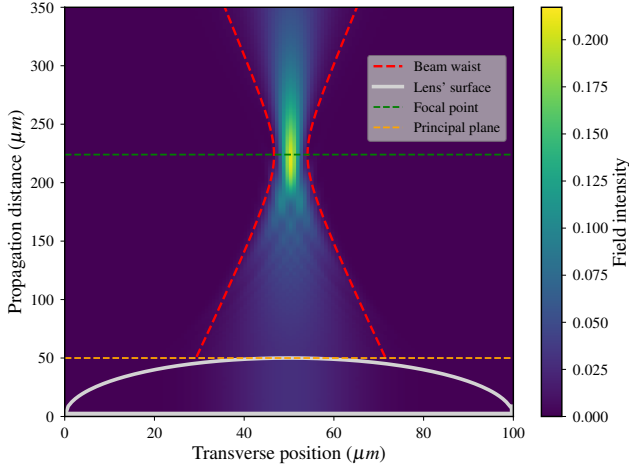
The relations in Eq. (B17) and Eq. (B18) are used in the analysis of the performance of the simulation in Section IV.

### Appendix C: Simulation of various cases and orientations of lenses

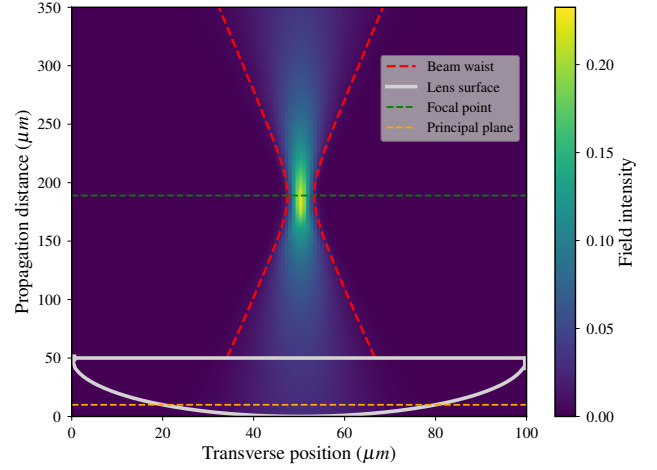
In this section, we present additional lens simulations using the presented quantum algorithm to showcase the flexibility of the block-encoding technique for simulating different optical experiments. In wave optics [36], it is known that the focusing performance of a lens with a finite thickness depends on its shape and geometry, namely the radii of curvature of its surfaces and the orientation of the lens.

To see these effects, we simulated four different cases. We started with a spherical lens in the orientation where the beam hits the planar surface first (Fig. 1a) and then simulated the same lens but in the reverse orientation (Fig. 1b). And then instead of the lens with a spherical surface, we approximated the curved surface by a parabolic curvature and repeated the simulation in both orientations (Fig. 1c and 1d). The parabolic approximation is chosen such that the curvature at the optical axis is the same for the spherical and parabolic lenses which means the parabolic lens will generally have a smaller surface curvature at other points on its surface compared to the spherical lens. The general scheme of the simulations is exactly the same as described in Section IV of the main manuscript and the only change is the different phases applied to the incident beam by the lens based on its shape and orientation.

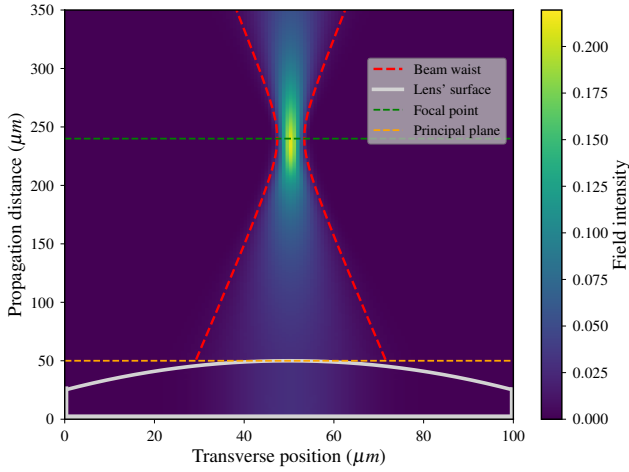
Several effects are expected from and seen in these simulations. It is known [36] that the orientation of the lens where the beam hits the curved surface first is considered the ‘‘better’’ orientation because the focusing power is distributed on both surfaces; whereas in the other orientation, it is only the curved surface which contributes to the refraction. This leads to two effects. First, the ‘‘bad’’ orientation potentially leads to more prominent aberration effects because it amplifies the spherical aberrations relatively more. Second, there will be a shift of the focal point because the principal plane (approximate effective position of the focusing plane if we approximate the lens as a thin



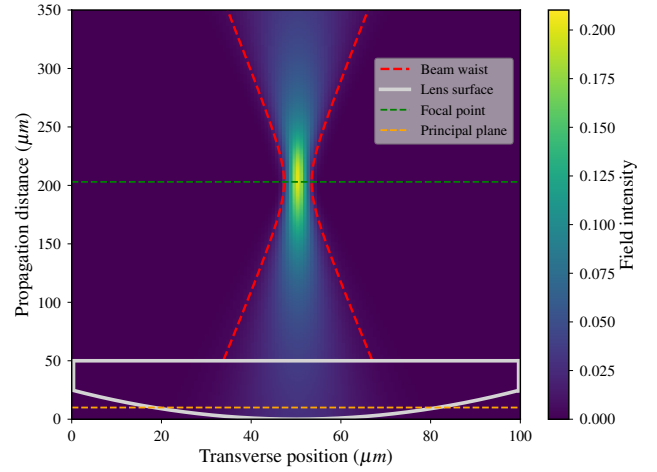
(a) Spherical lens, “bad” orientation



(b) Spherical lens, “good” orientation



(c) Parabolic lens, “bad” orientation



(d) Parabolic lens, “good” orientation

FIG. 1: Simulation results of focusing a gaussian beam incident on various lenses. The simulation parameters are: the wavelength, initial gaussian beam waist, refractive index, radius of curvature (at optical axis), and number of qubits, respectively  $\lambda = 1\mu m$ ,  $w_0 = 25\mu m$ ,  $n = 1.25$ ,  $R = 50\mu m$ , and  $n_q = 7$ .

lens) has different positions depending on the orientation. Comparing the spherical and parabolic lenses in a fixed orientation, we can also see that the focal distance is effectively larger in the parabolic case because of the smaller effective curvature of the parabolic approximation. A parabolic lens also reduces the spherical aberrations for the gaussian beam input. This shows that the simulation protocol presented in this work offers an intuitive way to run various optical simulations using a quantum computer.

- 
- [1] A. J. Daley, I. Bloch, C. Kokail, S. Flannigan, N. Pearson, M. Troyer, and P. Zoller, Practical quantum advantage in quantum simulation, *Nature* **607**, 667 (2022).
- [2] E. Altman, K. R. Brown, G. Carleo, L. D. Carr, E. Demler, C. Chin, B. DeMarco, S. E. Economou, M. A. Eriksson, K.-M. C. Fu, M. Greiner, K. R. Hazzard, R. G. Hulet, A. J. Kollár, B. L. Lev, M. D. Lukin, R. Ma, X. Mi, S. Misra, C. Monroe, K. Murch, Z. Nazario, K.-K. Ni, A. C. Potter, P. Roushan, M. Saffman, M. Schleier-Smith, I. Siddiqi, R. Simmonds, M. Singh, I. Spielman, K. Temme, D. S. Weiss, J. Vučković, V. Vuletić, J. Ye, and M. Zwierlein, Quantum Simulators: Architectures and Opportunities, *PRX Quantum* **2**, 017003 (2021).
- [3] S. Pirandola, U. L. Andersen, L. Banchi, M. Berta, D. Bunandar, R. Colbeck, D. Englund, T. Gehring, C. Lupo, C. Ot-

- taviani, J. L. Pereira, M. Razavi, J. S. Shaari, M. Tomamichel, V. C. Usenko, G. Vallone, P. Villoresi, and P. Wallden, Advances in quantum cryptography, *Advances in Optics and Photonics* **12**, 1012 (2020).
- [4] M. Cerezo, G. Verdon, H.-Y. Huang, L. Cincio, and P. J. Coles, Challenges and opportunities in quantum machine learning, *Nature Computational Science* **2**, 567 (2022).
- [5] A. M. Dalzell, S. McArdle, M. Berta, P. Bienias, C.-F. Chen, A. Gilyén, C. T. Hann, M. J. Kastoryano, E. T. Khabiboulline, A. Kubica, G. Salton, S. Wang, and F. G. S. L. Brandão, *Quantum Algorithms: A Survey of Applications and End-to-end Complexities* (Cambridge University Press, Cambridge, 2025).
- [6] R. Santagati, A. Aspuru-Guzik, R. Babbush, M. Degroote, L. González, E. Kyoseva, N. Moll, M. Oppel, R. M. Parrish, N. C. Rubin, M. Streif, C. S. Tautermann, H. Weiss, N. Wiebe, and C. Utschig-Utschig, Drug design on quantum computers, *Nature Physics* **20**, 549 (2024).
- [7] D. Herman, C. Googin, X. Liu, Y. Sun, A. Galda, I. Safro, M. Pistoia, and Y. Alexeev, Quantum computing for finance, *Nature Reviews Physics* **5**, 450 (2023).
- [8] A. Di Meglio, K. Jansen, I. Tavernelli, C. Alexandrou, S. Arunachalam, C. W. Bauer, K. Borrás, S. Carrazza, A. Crippa, V. Croft, R. de Putter, A. Delgado, V. Dunjko, D. J. Egger, E. Fernández-Combarro, E. Fuchs, L. Funcke, D. González-Cuadra, M. Grossi, J. C. Halimeh, Z. Holmes, S. Kühn, D. Lacroix, R. Lewis, D. Lucchesi, M. L. Martinez, F. Meloni, A. Mezzacapo, S. Montangero, L. Nagano, V. R. Pascuzzi, V. Radescu, E. R. Ortega, A. Roggero, J. Schuhmacher, J. Seixas, P. Silvi, P. Spentzouris, F. Tacchino, K. Temme, K. Terashi, J. Tura, C. Tüysüz, S. Vallecorsa, U.-J. Wiese, S. Yoo, and J. Zhang, Quantum Computing for High-Energy Physics: State of the Art and Challenges, *PRX Quantum* **5**, 037001 (2024).
- [9] G. Mazzola, Quantum computing for chemistry and physics applications from a Monte Carlo perspective, *The Journal of Chemical Physics* **160**, 010901 (2024).
- [10] R. P. Feynman, Simulating physics with computers, *International Journal of Theoretical Physics* **21**, 467 (1982).
- [11] S. Lloyd, Universal Quantum Simulators, *Science* **273**, 1073 (1996).
- [12] I. Georgescu, S. Ashhab, and F. Nori, Quantum simulation, *Reviews of Modern Physics* **86**, 153 (2014).
- [13] A. W. Harrow, A. Hassidim, and S. Lloyd, Quantum Algorithm for Linear Systems of Equations, *Physical Review Letters* **103**, 150502 (2009).
- [14] D. W. Berry, High-order quantum algorithm for solving linear differential equations, *Journal of Physics A: Mathematical and Theoretical* **47**, 105301 (2014).
- [15] P. Webster, M. Vasmer, T. R. Scruby, and S. D. Bartlett, Universal fault-tolerant quantum computing with stabilizer codes, *Physical Review Research* **4**, 013092 (2022).
- [16] R. Toshio, Y. Akahoshi, J. Fujisaki, H. Oshima, S. Sato, and K. Fujii, Practical Quantum Advantage on Partially Fault-Tolerant Quantum Computer, *Physical Review X* **15**, 021057 (2025).
- [17] F. Battistel, C. Chamberland, K. Johar, R. W. J. Overwater, F. Sebastiano, L. Skoric, Y. Ueno, and M. Usman, Real-time decoding for fault-tolerant quantum computing: progress, challenges and outlook, *Nano Futures* **7**, 032003 (2023).
- [18] E. T. Campbell, B. M. Terhal, and C. Vuillot, Roads towards fault-tolerant universal quantum computation, *Nature* **549**, 172 (2017).
- [19] A. M. Childs and N. Wiebe, Hamiltonian simulation using linear combinations of unitary operations, *Quantum Information and Computation* **12**, 901 (2012).
- [20] G. H. Low and I. L. Chuang, Hamiltonian Simulation by Qubitization, *Quantum* **3**, 163 (2019).
- [21] A. Gilyén, Y. Su, G. H. Low, and N. Wiebe, Quantum singular value transformation and beyond: exponential improvements for quantum matrix arithmetics, in *Proceedings of the 51st Annual ACM SIGACT Symposium on Theory of Computing, STOC 2019* (Association for Computing Machinery, New York, NY, USA, 2019) pp. 193–204.
- [22] J. M. Martyn, Z. M. Rossi, A. K. Tan, and I. L. Chuang, Grand Unification of Quantum Algorithms, *PRX Quantum* **2**, 040203 (2021).
- [23] J. D. Schmidt, J. A. Tellez, and G. J. Gbur, Semi-analytic simulation of optical wave propagation through turbulence, *Applied Optics* **61**, 9439 (2022).
- [24] R. Heintzmann, L. Loetgering, and F. Wechsler, Scalable angular spectrum propagation, *Optica* **10**, 1407 (2023).
- [25] M. Wende, J. Drozella, A. Toulouse, and A. M. Herkommer, Fast vector wave optical simulation methods for application on 3D-printed microoptics, *Journal of Optical Microsystems* **4**, 024501 (2024).
- [26] Y. Liu, F. Guo, Z. Zhang, and R. Wu, Wave optical propagation in realistic lens systems through multi-slice decomposition with phase compensation, *Applied Optics* **63**, F18 (2024).
- [27] Y. Sung, B. Nelson, and R. Gupta, Realistic wave-optics simulation of X-ray dark-field imaging at a human scale, *Scientific Reports* **15**, 26748 (2025).
- [28] J. Lu, D. Qu, J. Qu, R. Fong, G. H. Ahn, and J. Vuckovic, A systolic update scheme to overcome memory bandwidth limitations in GPU-accelerated FDTD simulations (2025), arXiv:2502.20610 [physics].
- [29] Z. Wu, Y. You, X. Zhou, and F. Zhang, Accelerated time-domain simulation of complex photonic structures with a Data-Aware Fourier Neural Operator, *Optics Communications* **604**, 132838 (2026).
- [30] R. Shams and P. Sadeghi, On optimization of finite-difference time-domain (FDTD) computation on heterogeneous and GPU clusters, *Journal of Parallel and Distributed Computing* **71**, 584 (2011).
- [31] B. D. Clader, B. C. Jacobs, and C. R. Sprouse, Preconditioned Quantum Linear System Algorithm, *Physical Review Letters* **110**, 250504 (2013).
- [32] C. Cholsuk, S. Davani, L. O. Conlon, T. Vogl, and F. Eilenberger, Efficient light propagation algorithm using quantum computers, *Physica Scripta* **99**, 045110 (2024).
- [33] J. S. Kottmann, M. Krenn, T. H. Kyaw, S. Alperin-Lea, and A. Aspuru-Guzik, Quantum computer-aided design of quantum

- optics hardware, *Quantum Science and Technology* **6**, 035010 (2021).
- [34] J. M. Burzler, S. Hughes, and B. S. Wherrett, Split-step fourier methods applied to model nonlinear refractive effects in optically thick media, *Applied Physics B* **62**, 389 (1996).
  - [35] M. A. Nielsen and I. L. Chuang, *Quantum Computation and Quantum Information: 10th Anniversary Edition*, 1st ed. (Cambridge University Press, 2012).
  - [36] B. E. A. Saleh and M. C. Teich, *Fundamentals of Photonics*, 1st ed. (Wiley, 1991).
  - [37] H. F. Trotter, On the product of semi-groups of operators, *Proceedings of the American Mathematical Society* **10**, 545 (1959).
  - [38] X. Yang, X. Nie, Y. Ji, T. Xin, D. Lu, and J. Li, Improved quantum computing with higher-order Trotter decomposition, *Physical Review A* **106**, 042401 (2022).
  - [39] M. Kieferová, A. Scherer, and D. W. Berry, Simulating the dynamics of time-dependent Hamiltonians with a truncated Dyson series, *Physical Review A* **99**, 042314 (2019).
  - [40] S.-J. Ran, Encoding of matrix product states into quantum circuits of one- and two-qubit gates, *Physical Review A* **101**, 032310 (2020).
  - [41] J. Iaconis, S. Johri, and E. Y. Zhu, Quantum state preparation of normal distributions using matrix product states, *npj Quantum Information* **10**, 1 (2024).
  - [42] M. Schuld and F. Petruccione, Representing Data on a Quantum Computer, in *Machine Learning with Quantum Computers*, edited by M. Schuld and F. Petruccione (Springer International Publishing, Cham, 2021) pp. 147–176.
  - [43] A. Gilyén, S. Arunachalam, and N. Wiebe, Optimizing quantum optimization algorithms via faster quantum gradient computation, in *Proceedings of the 2019 Annual ACM-SIAM Symposium on Discrete Algorithms (SODA)*, Proceedings (Society for Industrial and Applied Mathematics, 2019) pp. 1425–1444.